Design of pedestal disk resonators in $KY(WO_4)_2$ for Kerr frequency combs

S. M. Martinussen, R. N. Frentrop, S. M. Garcia-Blanco

University of Twente, MESA+ Institute for Nanotechnology, Optical Sciences Group, P.O. Box 217, 7500 AE Enschede, The Netherlands

In this work we explore the design of pedestal disk resonators in $KY(WO_4)_2$ for use as Kerr frequency combs. Such disks can be fabricated by a combination of sub-surface amorphization through swift carbon ion irradiation, deep focused ion beam etching, and a wet etch step that selectively dissolves the amorphized material. We explore the device geometries that will optimize performance towards efficient frequency comb generation and consider the influence of important fabrication parameters. Special consideration is given to avoiding overlap of cavity modes and Raman peaks, in order to avoid stimulated Raman scattering outcompeting Kerr gain.

Introduction

$KY(WO_4)_2$, hereafter KYW, has long been in use for bulk lasers [1] thanks to its excellent properties as a rare earth ion host [2]. In recent years, KYW has also been used for waveguide lasers [3] and amplifiers [4]. A strong Raman gain of 5.1 cm/GW [5] at 1064 nm makes KYW a very attractive material for Raman lasing.

However, the material still has untapped potential. Past devices have mostly been based on epitaxially grown layers with a low refractive index contrast of $\sim 10^{-2}$ [6]. This causes low modal confinement, restricts the devices to straight waveguides and makes dispersion engineering difficult. For this reason, the high Kerr nonlinearity of $n_2 = 1.5\times10^{-19}$ m^2/W at 819 nm [7] of the material has not yet been exploited.

Increasing the refractive index contrast between KYW and the substrate can remove the limitations mentioned. To this end, swift carbon ion irradiation is used to create a reduced-index, amorphized layer below the surface [8]. After a thermal annealing step that reduces point defects and steepens the step-like shape of the index profile, the surface layer is mostly crystalline and acts as a slab waveguide, with an index contrast of ~0.2 to the amorphized layer. The slab can be further structured by focused ion beam milling [9]. A highly selective wet etch allows for removal of the amorphized layer with little damage to the crystalline layer, forming pedestal structures [9].

This study deals with the design of a disk resonator for Kerr frequency comb applications. Kerr frequency combs are a compact alternative to mode locked lasers for ultrastable microwave generation [10], precision distance measurements [11] and other applications. The problem is approached by investigating two topics: First, the effects of the device geometry on its performance. Second, the feasibility of a purely Kerr driven device, in contrast with a device combining Raman and Kerr effects.

Geometry and dispersion engineering

Mode simulations in Lumerical MODE Solutions were used to investigate the effects of the disk geometry. The disk radius and the thickness of an optional SiO_2 cladding were under consideration, as illustrated in Figure 1.

The effect of these parameters on the group index, device losses, and effective mode area were investigated at a wavelength of 1550 nm. The group index n_g is important as it links the free spectral range (FSR) and resonator size through the relation $FSR = c/(4\pi r n_g)$. The losses are also important, as they determine the Q factor. The effective mode area A_{eff} is

proportional to the threshold power needed to generate a comb, $P_{th} = \frac{\omega_L n_0^2 A_{eff} L}{4cn_2 Q^2}$ [12], and should thus be minimized. The dispersion in the wavelength range 1 µm to 2 µm was also simulated in order to directly examine how the zero-dispersion wavelength (ZDW) changes depending on the device geometry.

The initial parameters were based on a FIB milled disk with vertical sidewalls. Complete removal of the amorphized layer under the core and a vertical sidewall are assumed, based on previous devices [9]. Such complete removal is desirable, as the amorphized region induces losses [8]. The remaining core has a thickness of 1.2 µm, the default disk radius was 4 µm and only one parameter was changed at a time, while the other remained as in the default structure.

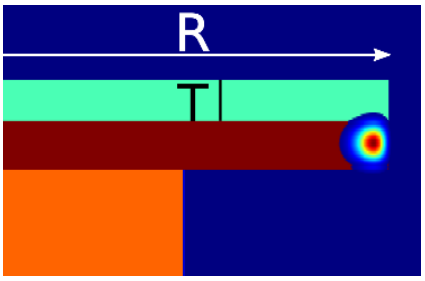

Figure 1: The refractive index profile of the disk structure with the fundamental TM mode superimposed. The SiO_2 cladding (green) thickness is indicated by T, the radius by R. The core (red) thickness is 1.2 µm. The amorphized layer is orange.

Effect of bend radius and cladding thickness

The bend radius was varied between 3 µm and 100 µm. It was found that the radius has a great impact on the device performance. The mode area A_{eff} decreases from 2 µm^2 at a radius of 100 µm to 0.76 µm^2 at 4 µm. The effects of bend radius on A_{eff} is shown in Figure 2 a. The group index increases with increasing radius, from 1.92 to 2.04 at 4 µm and 100 µm respectively. The dispersion is also dependent on the radius. At 4 µm radius the ZDW is around 1470 nm, at 10 µm it is 1275 nm and at 100 µm it is down to 1150 nm.

Bend losses also come into play. The simulated losses are only 0.007 dB/cm at 4 µm radius, but reach 0.98 dB/cm at 3 µm radius. While the threshold power is proportional to the mode area and disk radius [12], it is inversely proportional to Q^2, which is dependent

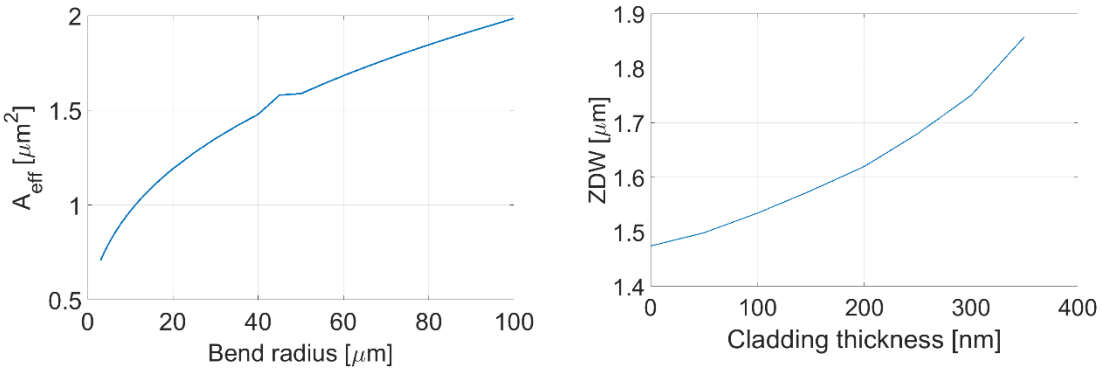

Figure 2: a: Bend radius vs effective mode area of the fundamental TM mode. A small disk has a drastically smaller mode than a large disk due to the mode being confined to the disk edge. The bump at 45 µm is caused by a local increase in TE polarization as the TM_0 and TE_1 modes obtain similar n_{eff}.
b: Cladding thickness vs zero-dispersion wavelength. The zero-dispersion wavelength becomes longer than the limits of the simulation when the thickness grows above 350 nm.

on the losses. However, a wide anomalous dispersion region will increase the comb span. This, along with a closer mode spacing that provides better phase matching, is an argument in favor of larger disks.

The SiO_2 cladding thickness was varied between 0 µm and 1 µm. The biggest change is a significant increase in the ZDW, shown in Figure 2 b, which goes above 2 µm for cladding thicknesses of more than 350 nm. Thus, the cladding should be removed.

The losses cannot be accurately predicted as they will likely be dominated by scattering, which depends on fabrication results and cannot be simulated. However, assuming a Q factor of 10^5, calculated from a 1 dB/cm loss, and a radius of 4 µm yields a threshold power of 23 mW.

Minimizing the influence of Raman gain

Designing for Kerr nonlinearity in a Raman active medium requires special considerations, as the Raman gain g_R may outcompete the Kerr gain g_K and destabilize the mode-locking process [13]. This increases the complexity of the nonlinear interactions [14] and can limit the comb's usefulness for applications that require a periodic, coherent pulse train, like microwave generation [15] and precision distance measurements [11]. However, under specific conditions it can be possible to generate coherent combs at both the pump and Stokes wavelengths [14].
In one approach, Okawachi et al. [13] minimized Raman gain by requiring that g_K must be higher than the g_R at all cavity modes. Under the condition of narrowband Raman gain, a lower limit to the FSR can be calculated from the Raman peak width and the g_R/g_K ratio. Since the Raman gain spectrum for KYW is broadband, shown in Figure 2, this analysis is insufficient for KYW. The Raman scattering spectrum is based on measurements performed in a previous work [16]. This spectrum is scaled to the 905 cm^{-1} gain peak of g_R = 5.1 cm/GW [5], as the peak scattering determines the stimulated Raman gain [17].
A direct approach to finding a working design consists of generating periodic comb lines and checking if they overlap with the regions where $g_R > g_K$. A pump wavelength of 1550 nm in $E||N_p$ polarization is considered, which corresponds to the crystal's b-axis [18]. Thilmann's n_2 value [7] is used, as experimental values are unavailable at longer wavelengths. The Kerr gain is given by $g_K = 2\pi n_2/\lambda$ [19].

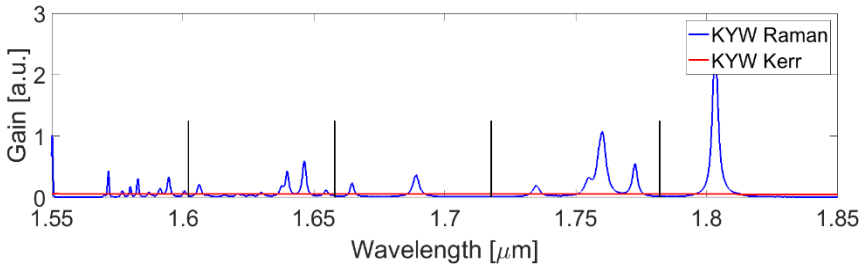

Figure 3: Raman and Kerr gain spectra of KYW for polarization along the b axis. The Raman spectrum has been shifted relative to a pump at 1550 nm. The black lines show the resonator modes for a 1.99 µm radius disk with no Raman dominated resonances..

Performing this analysis shows that there is no radius where a Raman-free comb can exist. However, these calculations have been performed using gain values measured at 1064 nm. The gain will be lower at longer wavelengths, but there is significant uncertainty concerning the actual number, as Raman gain values are not available in literature. Applying a λ^{-2} proportionality to the values given by Černý [5] yields g_R = 2.4 cm/GW at 1550 nm. This allows Raman-free combs of 1.98 µm ± 25 nm and 2.43 µm ± 20 nm radius, given a group index of 1.9. However, such a tight bend radius will cause radiation losses of around 10 dB/cm according to mode simulations. Furthermore, achieving phase matching will be challenging for such a high FSR. 3 shows the Raman gain, Kerr gain and position of the resonator modes for a 1.99 µm disk.

Discussion and conclusion

We have considered the design of a pedestal disk for Kerr frequency comb applications. It was found that to avoid overlap of resonator modes and Raman peaks, the disk radius is highly restricted. A radius near 2.46 μm fulfills this condition for a 1550 nm pump, but will suffer due to bend losses and normal dispersion. Accurate numbers for Raman and Kerr gain in mid-IR are needed for a firm conclusion, however an approach that aims to utilize both Raman and Kerr effects is likely to be more fruitful. Mode simulations indicate that the disk should have no cladding. This will maximize the span of the anomalous dispersion region and reduce losses, which is key to a broadband comb with low threshold power.

This project has received funding from the European Research Council (ERC) under the European Union's Horizon 2020 research and innovation programme under grant agreement No 648978.

[1] A. a. Kovalyov *et al.*, "115 fs pulses from Yb^{3+}:$KY(WO_4)_2$ laser with low loss nanostructured saturable absorber," *Laser Phys. Lett.*, vol. 8, no. 6, pp. 431–435, Jun. 2011.

[2] Y.-S. Yong *et al.*, "Direct confocal lifetime measurements on rare-earth-doped media exhibiting radiation trapping," *Opt. Mater. Express, OME*, vol. 7, no. 2, pp. 527–532, Feb. 2017.

[3] D. Geskus, S. Aravazhi, C. Grivas, K. Wörhoff, and M. Pollnau, "Microstructured $KY(WO_4)_2$:Gd^{3+}, Lu^{3+}, Yb^{3+} channel waveguide laser," *Optics Express*, vol. 18, no. 9, p. 8853, Apr. 2010.

[4] D. Geskus, S. Aravazhi, S. M. García-Blanco, and M. Pollnau, "Giant Optical Gain in a Rare-Earth-Ion-Doped Microstructure," *Adv. Mater.*, vol. 24, no. 10, pp. OP19–OP22, Mar. 2012.

[5] P. Černý, P. G. Zverev, H. Jelínková, and T. T. Basiev, "Efficient Raman shifting of picosecond pulses using $BaWO_4$ crystal," *Optics Communications*, vol. 177, no. 1, pp. 397–404, Apr. 2000.

[6] S. Aravazhi *et al.*, "Engineering lattice matching, doping level, and optical properties of $KY(WO_4)_2$:Gd, Lu, Yb layers for a cladding-side-pumped channel waveguide laser," *Appl. Phys. B*, vol. 111, no. 3, pp. 433–446, May 2013.

[7] N. Thilmann, G. Strömqvist, M. C. Pujol, V. Pasiskevicius, V. Petrov, and F. Díaz, "Nonlinear refractive indices in Yb^{3+}-doped and undoped monoclinic double tungstates $KRE(WO_4)_2$ where RE=Gd, Y, Yb, Lu," *Appl. Phys. B*, vol. 96, no. 2–3, pp. 385–392, Aug. 2009.

[8] R. Frentrop, M. Dijkstra, V. Tormo-Marquez, J. Olivares, and S. Garcia-Blanco, "High-contrast slab waveguide fabrication in $KY(WO_4)_2$ by swift heavy ion irradiation," presented at the Integrated Optics: Devices, Materials, and Technologies XXII, 2018.

[9] S. M. Martinussen *et al.*, "Pedestal disk resonator in potassium yttrium double tungstate," in *Integrated Optics: Devices, Materials, and Technologies XXII*, 2018, vol. 10535, p. 105350Q.

[10] S. A. Diddams *et al.*, "Direct Link between Microwave and Optical Frequencies with a 300 THz Femtosecond Laser Comb," *Phys. Rev. Lett.*, vol. 84, no. 22, pp. 5102–5105, May 2000.

[11] M.-G. Suh and K. J. Vahala, "Soliton microcomb range measurement," *Science*, vol. 359, no. 6378, pp. 884–887, Feb. 2018.

[12] G. Lin, A. Coillet, and Y. K. Chembo, "Nonlinear photonics with high-Q whispering-gallery-mode resonators," *Adv. Opt. Photon., AOP*, vol. 9, no. 4, pp. 828–890, Dec. 2017.

[13] Y. Okawachi *et al.*, "Competition between Raman and Kerr effects in microresonator comb generation," *Opt. Lett., OL*, vol. 42, no. 14, pp. 2786–2789, Jul. 2017.

[14] Y. K. Chembo, I. S. Grudinin, and N. Yu, "Spatiotemporal dynamics of Kerr-Raman optical frequency combs," *Phys. Rev. A*, vol. 92, no. 4, p. 043818, Oct. 2015.

[15] W. Liang *et al.*, "High spectral purity Kerr frequency comb radio frequency photonic oscillator," *Nature Communications*, vol. 6, p. 7957, Aug. 2015.

[16] R. N. Frentrop et al., "Emergence of new crystalline phase in high temperature annealed, carbon irradiated α-$KY(WO_4)_2$," in *IEEE Photonics Benelux Proceedings*, 2017, pp. 136–196.

[17] R. W. Boyd, *Nonlinear optics*. Amsterdam ; Academic Press, 2008.

[18] X. Mateos et al., "Crystal growth, optical and spectroscopic characterisation of monoclinic $KY(WO_4)_2$ co-doped with Er^{3+} and Yb^{3+}," *Optical Materials*, vol. 28, no. 4, pp. 423–431, Mar. 2006.

[19] G. P. Agrawal, *Nonlinear Fiber Optics*. Academic Press, 2013.